Pergamon

Int J. Solids Structures Vol. 31, No. 19, pp. 2709–2733, 1994
Elsevier Science Ltd
Printed in Great Britain
0020–7683/94 $7.00 + .00

0020–7683(94)E0053–X

ECHELON MODES IN UNIFORM MATERIALS

KIYOHIRO IKEDA
Department of Civil Engineering, Tohoku University, Aoba, Sendai 980, Japan

KAZUO MUROTA
Research Institute for Mathematical Sciences, Kyoto University, Kyoto 606, Japan

and

MASAKI NAKANO
Department of Civil Engineering, Nagoya University, Chigusa, Nagoya 464-01, Japan

(*Received* 24 *January* 1994)

Abstract—The mechanism of the "echelon" mode—a series of parallel short wrinkles of soils that looks like a flight of stairs or wild geese arranged in formation—observed in the triaxial compression test is revealed by means of the group-theoretic bifurcation theory. The study of the direct bifurcation of uniform materials in cylindrical domains with periodic boundaries has revealed the existence of various kinds of deformation patterns. In particular, a classical diamond (checkerboard) pattern solution and a pair of "oblique" stripe pattern solutions simultaneously branch at a bifurcation point of multiplicity four. With the use of the periodic boundaries these oblique stripe solutions, which cannot be directly obtained by the customary bifurcation analysis with non-periodic boundaries, have thus been made accessible. The secondary bifurcation from these stripe solutions realizes the "echelon" mode. The triaxial compression tests on soil specimens have demonstrated that the pattern of wrinkles, shear bands and echelon modes of the specimens do indeed follow the present theory, and can be understood as a natural consequence of pattern selection, or, in other words, symmetry-breaking bifurcation.

1. INTRODUCTION

The simulation of shear-band formation behavior of soils, rocks and other materials is well known to entail some essential difficulties although its various phenomenological aspects have been well understood through diversified research. The method of plastic bifurcation has long been accepted as a theoretical basis for the formation of shear bands [see, e.g. Hill and Hutchinson (1975) and Vermeer (1982)]. The inherent and induced anisotropies have come to be acknowledged as a major source of complex material properties [see, e.g. Sekiguchi and Ohta (1977)]. The finite-element simulation of shear band formation is showing some success [see, e.g. Prevost (1984) and Yatomi *et al.* (1989a, b)]. The concept of imperfection sensitivity was used to show the presence of bifurcation in the triaxial compression test of sand specimens (Ikeda and Goto, 1993). Thus "bifurcation" seems to be a promising course of future study on that behavior.

A shear band of cylindrical soil specimens observed in triaxial compression tests is often made up of a series of oblique parallel short wrinkles arranged with similar intervals as shown in Fig. 1; the shear band and the wrinkles are directed in completely different directions. In the field of structural geology, this is called an "echelon mode", which means the pattern of a flight of stairs or wild geese arranged in formation.

Such a mode can be found elsewhere. An echelon crack in granite also exhibits similar features, as shown in Fig. 2 (Petit, 1988). The photograph and the sketch of the ductile shear zones of halite (cooking salt) shown in Fig. 3 (Shimamoto, 1989), which was used to develop a fault-zone model, are characterized by wavy-shaped foliation with fine intervals shown by solid lines, and fairly sharp oblique discontinuities with coarse intervals shown by heavy solid lines. These discontinuities appear to be arranged parallel. To sum up, all these diversified materials with different physical properties are similar in that they all form

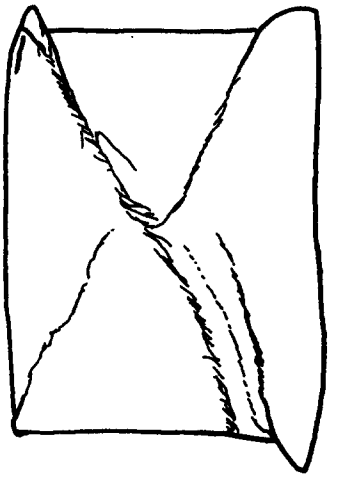

Fig. 1. An echelon mode on a cylindrical soil specimen.

echelon modes or stripe patterns. Such phenomenological similarity will imply the existence of an underlying general rule.

By contrast, in the fields of fluid mechanics, non-linear mathematics, and so on, it is well known that patterns are selected through recursive bifurcation which "breaks" symmetry. The Taylor–Couette flow in a hollow cylinder, which is a rotating annular of fluid, displays wave patterns with various kinds of symmetries through pattern selection [see, e.g. Taylor (1923)]. The convective motion of fluid, the so-called Benard problem, often displays a regularly arrayed (hexagonal) cellular structure [see, e.g. Koschmieder (1974)]. Cylindrical shells are noted to display various kinds of patterns, as shown in Fig. 4 (Yamaki, 1920). In particular, the pattern in Fig. 4(a) stands for the famous "diamond" pattern, while that in Fig. 4(b) presumably for the stripe pattern. Shells with regular polygonal symmetry collapse through recursive symmetry-breaking bifurcation [see, e.g. Ikeda *et al.* (1991)].

The major hypothesis of this paper is that the echelon modes in uniform materials are formed through the repeated occurrence of symmetry-breaking bifurcation, and hence can be dealt with by means of a unified strategy. Such bifurcation has been described successfully by the group-theoretic bifurcation theory, with an emphasis on its qualitative aspects [see, e.g. Sattinger (1979), Golubitsky and Schaeffer (1985) and Golubitsky *et al.* (1988)]. With reference to the symmetry of the system under consideration, the possible types of critical points and bifurcated solutions can be revealed, and the behavior of these solutions in the vicinity of these points can be thoroughly investigated by the Lyapounov–Schmidt decomposition.

One of the most important findings of this theory is that the structure (rule) of such bifurcation does not depend on the individual material or physical properties but merely on the symmetry of the system to be considered. We can find a group G that labels its symmetry, and a nested set of subgroups

$$G \rightarrow G_1 \rightarrow G_2 \rightarrow \cdots \tag{1}$$

that characterizes the hierarchical bifurcation structure. Here $\rightarrow$ denotes the process of bifurcation, and G_i $(i = 1, 2, \ldots)$ stand for the subgroups of G that label the reduced symmetry of the bifurcated solutions. The knowledge of such a bifurcation structure will be vital in the complete description of bifurcation behavior of uniform materials.

The aim of this paper is to advance, through an application and reorganization of these results hitherto developed in the group-theoretic bifurcation theory, a qualitative theory for describing various phenomenological aspects of the echelon modes for uniform materials. It is well known that the bifurcation modes obtained by the customary bifurcation analysis with non-periodic boundaries will not yield stripe patterns but harmonic modes, such as

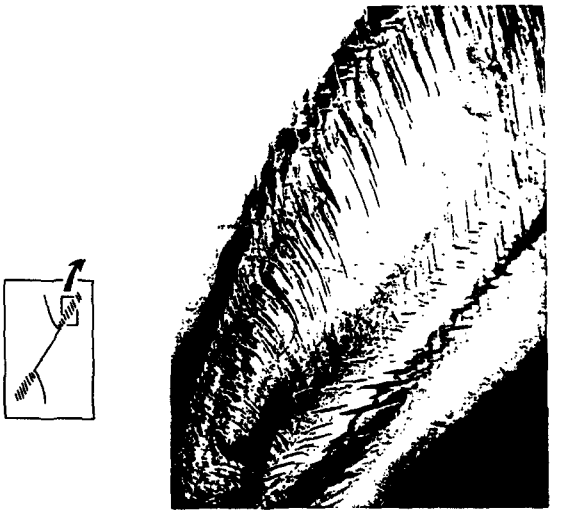

Fig. 2. Ductile shear zone with an echelon microcrack developed in PMMA (uniaxial loading test). Reprinted from Petit (1988) *Tectonics* 7, 1243–1256, copyright by the American Geophysical Union.

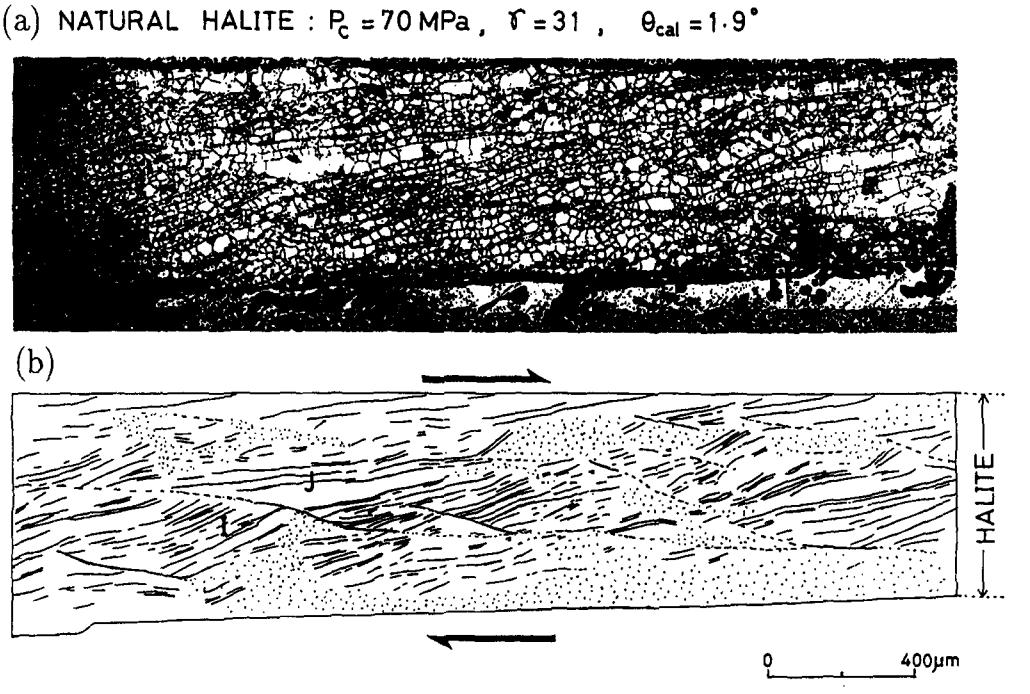

Fig. 3. Heterogeneous deformation showing distorted foliation (P_c = 70 Mpa, γ = 31). (a) Photograph. (b) Sketch showing foliation in solid lines, fairly sharp discontinuities in heavy solid lines, and structureless portion in dots. Reprinted from Shimamoto (1989).

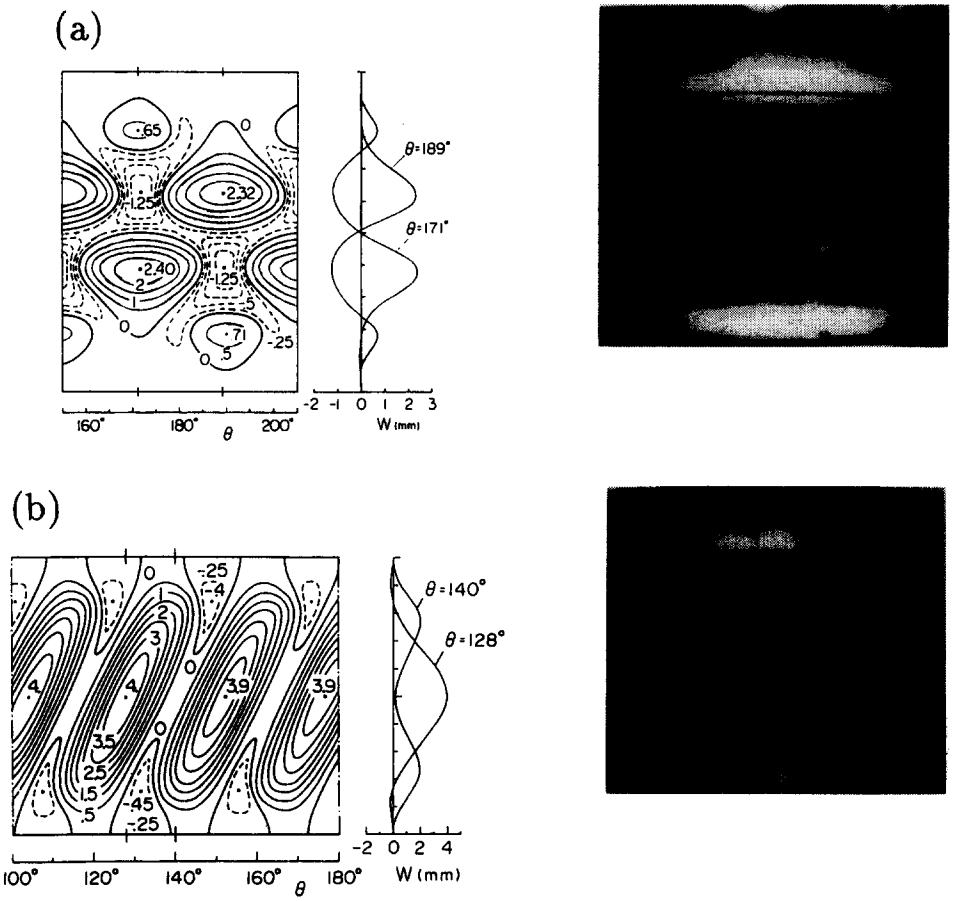

Fig. 4. Buckling patterns of cylinders; contour maps in the left and photographs in the right. (a) Diamond pattern. (b) Oblique stripe pattern. Reprinted from Yamaki (1920).

the diamond patterns. This indeed causes an essential difficulty in the simulation of the echelon modes made up of oblique stripes. In order to resolve this difficulty, we consider a cylindrical domain with the periodic boundary conditions at the ends so as to model translational symmetries in the axial direction. Then the symmetry group of this domain is defined with reference to its reflectional, rotational and periodic symmetries. The main (fundamental) equilibrium path for the system of governing equations of such domain retains its symmetry until reaching a (symmetry-breaking) bifurcation point, the multiplicity of which is shown to be one, two or four. The symmetries of possible bifurcated solutions for these bifurcation points are identified. In particular, for the point of multiplicity four, we have derived and solved the bifurcation equations to find that its possible bifurcated solutions consist of the classical diamond pattern (checkerboard) solution, and a pair of oblique stripe pattern solutions. The use of the periodic boundary conditions thus made these stripe patterns accessible as direct bifurcated solutions, and in turn has resolved one of the aforementioned essential difficulties in numerical simulation.

We have investigated the secondary bifurcation from the stripe pattern solutions to show the existence of a series of bifurcated solutions that represent the symmetries of echelon mode solutions. This recursive bifurcation realizes the mixture of oblique patterns with different directions and intervals to trigger induced anisotropies. The complexity of the recursive bifurcation is another essential difficulty in analysis.

We conducted extensive experiments on cylindrical soil specimens to thoroughly observe the emergence of wrinkles, shear bands and the echelon modes. It has been revealed that their patterns are selected in good agreement with the rule of the hierarchical recursive bifurcation by the present theory. The emergence of the echelon mode in soils has thus been understood as a natural consequence of the recursive bifurcation.

2. DEFORMATION PATTERNS IN CYLINDRICAL DOMAINS

As a preliminary stage of the study of bifurcation structure of uniform materials in a cylindrical domain, we shall explain how the symmetries of the deformation patterns of this domain are labeled by means of groups, and introduce a nested set of subgroups of eqn (1) that will lead to the echelon mode. Although we focus on the cylindrical domain in the remainder of this paper, the present formulation is easily modified for a rectangular domain as can be seen from Appendix A.

2.1. *Deformation pattern prior to bifurcation*

The cylindrical domain

$$\{(X, Y, Z) \mid X^2 + Y^2 \leqslant R_0(f), \quad 0 \leqslant Z \leqslant L(f)\}$$

of Fig. 5 is considered, where $R_0 = R_0(f)$ is the radius and $L = L(f)$ is the length of the

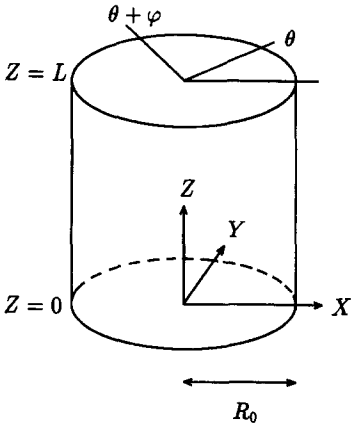

Fig. 5. Cylindrical domain.

cylinder, both of which may vary with the real-valued loading parameter f. In order to exclude the influence of the finiteness of this domain, we employ the *infinite cylinder approximation*, that is, the cylinder is assumed to have periodic boundary conditions on the top and the bottom surfaces at $Z = 0$ and $Z = L$. By virtue of this assumption, we can continuously extend this cylinder in the (axial) Z-direction to arrive at an imaginary, infinite and periodic cylinder. The use of this approximation, which is accurate away from the periodic boundaries, gives insight into the nature of deformation patterns in the middle of the cylinder. The cylinder consequently has symmetries in the circumferential and axial directions. Such combined symmetry can be expressed by a direct product

$$G = G_1 \times G_2$$

of the symmetry group G_1 for the circumferential symmetry and G_2 for the translational symmetry in the axial direction.

The circumferential (circular) symmetry can be characterized by the invariance under the counter-clockwise rotation $c(\varphi)$ around the Z-axis at an angle of φ $(0 \leqslant \varphi < 2\pi)$:

$$c(\varphi): \theta \mapsto \theta + \varphi, \tag{2}$$

[where $\theta = \tan^{-1}(Y/X)$] and the reflection σ_Y with respect to the XZ-plane:

$$\sigma_Y: Y \mapsto -Y \quad (\text{i.e. } \theta \mapsto -\theta). \tag{3}$$

The symmetry group G_1 for the circumferential symmetry is given by

$$C_{\infty v} = \langle \sigma_Y, c(\varphi) \rangle = \{c(\varphi), \sigma_Y c(\varphi) \mid 0 \leqslant \varphi < 2\pi\},$$

which is generated by $c(\varphi)$ (with $0 \leqslant \varphi < 2\pi$) and σ_Y. Here the brackets $\langle \cdot \rangle$ denote the group generated by the elements therein; the braces $\{\cdot\}$ denote the elements of the group; the product of elements, such as $\sigma_Y c(\varphi)$, denotes that the transformations are performed from the right to the left in sequence. The action of the element $\sigma_Y c(\varphi)$ is given by

$$\sigma_Y c(\varphi): \theta \mapsto -(\theta + \varphi),$$

and indicates the reflection with respect to the vertical plane that is perpendicular to the XY-plane and intersects with it at $\theta = -\varphi/2$.

The symmetry in the vertical direction can be characterized by the Z-directional translation $t(l)$ at a length of l $(0 \leqslant l < L)$ and the reflection σ_Z, being defined as:

$$t(l): Z \mapsto Z + l, \quad \sigma_Z: Z \mapsto -Z. \tag{4}$$

Hence G_2 is given by

$$\tilde{C}_{\infty v} = \langle \sigma_Z, t(l) \rangle = \{t(l), \sigma_Z t(l) \mid 0 \leqslant l < L\}.$$

The cylindrical domain, accordingly, is invariant under the group $C_{\infty v} \times \tilde{C}_{\infty v}$. It is noteworthy that the groups $C_{\infty v}$ and $\tilde{C}_{\infty v}$ are both isomorphic to a well-known group, which is conventionally denoted as $O(2)$ in the mathematical literature [that is, $G_1 \simeq G_2 \simeq O(2)$]. Some standard results, therefore, are available.

2.2. *Deformation patterns after bifurcation*

The subgroups of the symmetry group of a domain label the deformation patterns of the domain with reduced symmetries after bifurcation. We advance a series of typical patterns in the $(G =) C_{\infty v} \times \tilde{C}_{\infty v}$-invariant cylindrical domain and the subgroups of $C_{\infty v} \times \tilde{C}_{\infty v}$ that label their symmetries in the remainder of this subsection. It may be

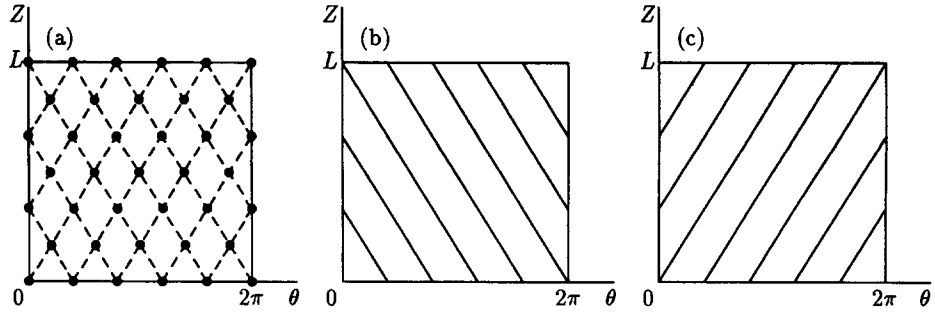

Fig. 6. Expansion plans of a series of patterns. (a) $DI_{n\tilde{n}}$-invariant diamond pattern ($n = 5$, $\tilde{n} = 3$). (b) $OB^{+}_{n\tilde{n}}$-invariant oblique stripe pattern ($n = 5$, $\tilde{n} = 3$). (c) $OB^{-}_{n\tilde{n}}$-invariant oblique stripe pattern ($n = 5$, $\tilde{n} = 3$). (●): Points with the same physical properties; straight lines: lines with the same physical properties.

emphasized here that the subgroups mentioned below do not exhaust all the subgroups of $C_{\infty v} \times \tilde{C}_{\infty v}$.

Figure 6(a) shows a diamond pattern in an expansion plan of the circumferential surface of the cylindrical domain, where the symbols (●) denote the points with the same physical properties, and the dashed lines are used to show the presence of diamond-shaped blocks with the same physical properties. This pattern is made up of a set of $n \times \tilde{n}$ identical diamond-shaped blocks arranged in order; furthermore, each block has upside-down, bilateral and half rotation symmetries. Here the half rotation refers to the in-plane rotation around the center of the domain at an angle of π. The pattern can be labeled by a group

$$DI_{n\tilde{n}} = \left\langle \sigma_Y, \sigma_Z, c\left(\frac{\pi}{n}\right)t\left(\frac{L}{2\tilde{n}}\right), c\left(\frac{\pi}{n}\right)t\left(\frac{-L}{2\tilde{n}}\right)\right\rangle. \tag{5}$$

Here the elements $c(\pi/n)t(\pm L/2\tilde{n})$ denote oblique translations at an angle of π/n in the circumferential direction and at a length of $\pm L/(2\tilde{n})$ in the vertical direction. These translations will move a diamond block to another, and hence will represent the symmetries of the diamond pattern. A harmonic function

$$\cos(n\theta)\cos\left(2\pi\tilde{n}\frac{Z}{L}\right) = \frac{1}{2}\left[\cos 2\pi\left(n\frac{\theta}{2\pi} + \tilde{n}\frac{Z}{L}\right) + \cos 2\pi\left(n\frac{\theta}{2\pi} - \tilde{n}\frac{Z}{L}\right)\right]$$

gives rise to an example of $DI_{n\tilde{n}}$-invariant pattern.

The stripe patterns, shown in Figs 6(b) and (c), have quite special symmetries labeled by a pair of groups

$$OB^{+}_{n\tilde{n}} = \left\langle \sigma_Y\sigma_Z, \left\{c(\varphi)t(l)\,\middle|\, n\frac{\varphi}{2\pi} + \tilde{n}\frac{l}{L} = N, \quad N = 0, \pm 1, \pm 2, \ldots\right\}\right\rangle, \tag{6}$$

$$OB^{-}_{n\tilde{n}} = \left\langle \sigma_Y\sigma_Z, \left\{c(\varphi)t(l)\,\middle|\, n\frac{\varphi}{2\pi} - \tilde{n}\frac{l}{L} = N, \quad N = 0, \pm 1, \pm 2, \ldots\right\}\right\rangle, \tag{7}$$

respectively. The elements $\{c(\varphi)t(l)\,|\,n(\varphi/2\pi) \pm \tilde{n}\,(l/L) = N\}$ (with N being integer numbers) indicate the invariance regarding arbitrary translation toward the direction of a series of oblique straight lines

$$n\frac{\theta}{2\pi} \pm \tilde{n}\frac{Z}{L} = N, \quad N = 0, \pm 1, \pm 2, \ldots$$

[shown by the straight lines in Figs 6(b) and (c)]. The material on these straight lines has the same physical properties. A pair of harmonic functions

$$\cos 2\pi \left(n\frac{\theta}{2\pi} \pm \tilde{n}\frac{Z}{L} \right)$$

gives rise to examples of $OB^{\pm}_{n\tilde{n}}$-invariant pattern, repectively.

The patterns shown in Fig. 7 will turn out to represent the echelon mode. A series of points (●) with the same physical properties often look like a number of oblique stripes that have different directions and intervals than the other stripes denoted by the dashed lines. This pattern is described by a finite subgroup of $C_{\infty v} \times \tilde{C}_{\infty v}$ defined by

$$EC^{+}_{n\tilde{n}kl} = \left\langle \sigma_Y \sigma_Z, c\left(-2\pi\frac{\tilde{n}}{dk}\right) t\left(L\frac{n}{dk}\right), c\left(\frac{2\pi}{d}\left(p - \frac{\tilde{n}l}{dk}\right)\right) t\left(\frac{L}{d}\left(\tilde{p} + \frac{nl}{dk}\right)\right) \right\rangle,$$

where n, $\tilde{n}$ and k are positive integers, d denotes the greatest common divisor of n and $\tilde{n}$, l is an integer with $0 \leqslant l \leqslant d-1$, and p and $\tilde{p}$ are integers such that $np + \tilde{n}\tilde{p} = d$. When n and $\tilde{n}$ are relatively prime (with $d = 1$), this expression reduces to

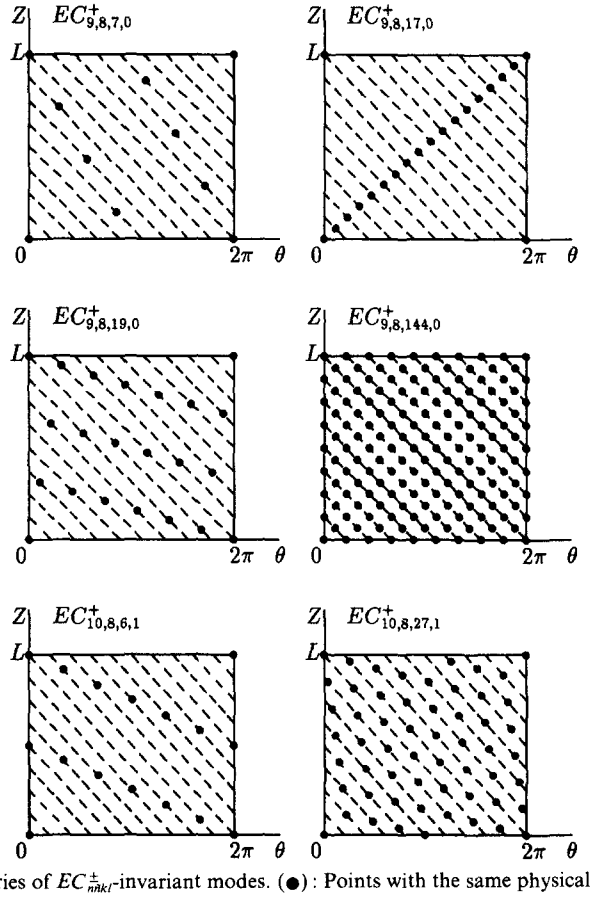

Fig. 7. A series of $EC^{\pm}_{n\tilde{n}kl}$-invariant modes. (●): Points with the same physical properties.

$$EC^{+}_{n\tilde{n}kl} = \left\langle \sigma_Y \sigma_Z, c\left(-2\pi\frac{\tilde{n}}{k}\right)t\left(L\frac{n}{k}\right)\right\rangle. \tag{8}$$

Similarly, we define

$$EC^{-}_{n\tilde{n}kl} = \left\langle \sigma_Y \sigma_Z, c\left(2\pi\frac{\tilde{n}}{dk}\right)t\left(L\frac{n}{dk}\right), c\left(\frac{2\pi}{d}\left(p+\frac{\tilde{n}l}{dk}\right)\right)t\left(\frac{L}{d}\left(\tilde{p}+\frac{nl}{dk}\right)\right)\right\rangle, \tag{9}$$

where p and $\tilde{p}$ are integers such that $np-\tilde{n}\tilde{p} = d$. Note that $EC^{+}_{n\tilde{n}kl}$ and $EC^{-}_{n\tilde{n}kl}$ are finite subgroups of $OB^{+}_{n\tilde{n}}$ and $OB^{-}_{n\tilde{n}}$, respectively, and contain $2dk$ elements. As we have seen in Fig. 7, $EC^{\pm}_{n\tilde{n}kl}$-invariant patterns vary greatly in association with the change in the values of the parameters k and l. The increase in k enhances the number of the points (●), which is equal to dk. The change in the values of l does not change their number but rearranges their location.

2.3. *Recursive loss of symmetry leading to echelon mode*

The major hypothesis propounded by the present paper is that the echelon mode is formed as a consequence of recursive loss of symmetry caused by recursive bifurcations. According to the theory to be developed in Section 3, the deformation pattern with $EC^{\pm}_{n\tilde{n}kl}$ symmetry cannot appear directly from the uniform deformation with $C_{\infty v}\times\tilde{C}_{\infty v}$ symmetry, but only by way of the stripe patterns with $OB^{\pm}_{n\tilde{n}}$ symmetry. For example,

$$C_{\infty v}\times\tilde{C}_{\infty v} \to OB^{\pm}_{n\tilde{n}} \to EC^{\pm}_{n\tilde{n}kl},$$

$$C_{\infty v}\times\tilde{C}_{\infty v} \to OB^{\pm}_{n\tilde{n}} \to OB^{\pm}_{m\tilde{m}} \to EC^{\pm}_{m\tilde{m}kl}$$

(where m and $\tilde{m}$ are integers satisfying $n/m = \tilde{n}/\tilde{m} \geqslant 2$) are possible sequences of nested subgroups leading to the $EC^{\pm}_{n\tilde{n}kl}$ (or $EC^{\pm}_{m\tilde{m}kl}$) symmetry.

At the early stage of deformation in association with the loss of symmetry

$$C_{\infty v}\times\tilde{C}_{\infty v} \to OB^{\pm}_{n\tilde{n}}$$

a set of oblique, parallel stripes is to be formed. Although these stripes may not be discernible at this stage, the material is weakened along the stripes. Then another oblique, parallel stripe pattern is to be formed in association with the loss of symmetry

$$OB^{\pm}_{n\tilde{n}} \to OB^{\pm}_{m\tilde{m}} \quad \text{or} \quad OB^{\pm}_{n\tilde{n}} \to EC^{\pm}_{n\tilde{n}kl}.$$

An example of this process is illustrated in Fig. 8. In the first case, the direction of the stripes (with the same physical properties) does not change but their interval enlarges. In the second case, on the other hand, the direction of the stripes (which are, precisely speaking, sequences of points) does change and their interval may enlarge or diminish.

The deformation patterns with $EC^{\pm}_{n\tilde{n}kl}$ symmetry may look different in individual cases. We offer in Fig. 9 three possible patterns: (a) a pattern in which stripes in another direction are just emerging (it is close to the pattern with $OB^{\pm}_{n\tilde{n}}$ symmetry); (b) a pattern in a transition made up of a pair of stripes with different directions and intervals; (c) an echelon mode characterized by coarse stripes each of which is made up of a series of parallel, fine short stripes. Although these three patterns appear different, they have the same symmetry labeled by $EC^{\pm}_{n\tilde{n}kl}$.

It is in order here to recall the echelon mode formation shown in Figs 1 and 2. A key to a correct qualitative interpretation of these phenomena is to know the correct sequence of the occurrence of a series of stripes. Intuitively since the fine short parallel wrinkles were observed along the line of the shear bands, etc. these wrinkles appear to be formed in association with the emergence of shear band, etc. Theoretically, the fine short wrinkles of

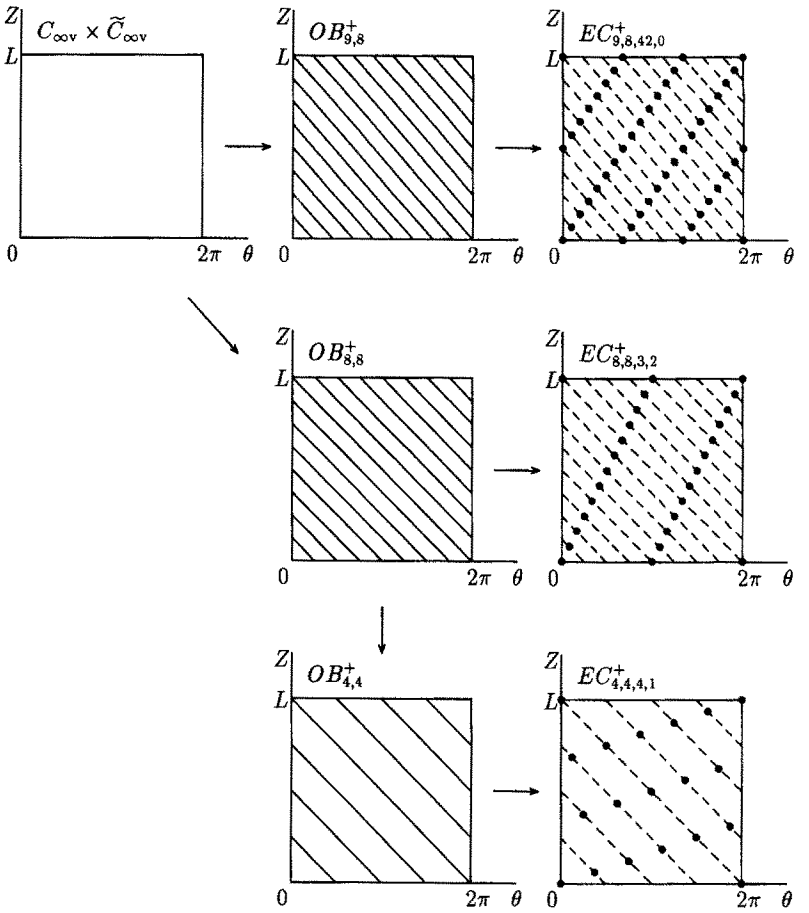

Fig. 8. Direction and interval change of stripe patterns through recursive loss of symmetry: $C_{\infty v} \times \tilde{C}_{\infty v} \to OB^{+}_{9,8} \to EC^{+}_{9,8,42,0}$, $C_{\infty v} \times \tilde{C}_{\infty v} \to OB^{+}_{8,8} \to EC^{+}_{4,4,3,2}$, $OB^{+}_{8,8} \to OB^{+}_{4,4} \to EC^{+}_{4,4,4,1}$ → : loss of symmetry due to bifurcation process; (●): points with the same physical properties; straight lines: lines with the same physical properties.

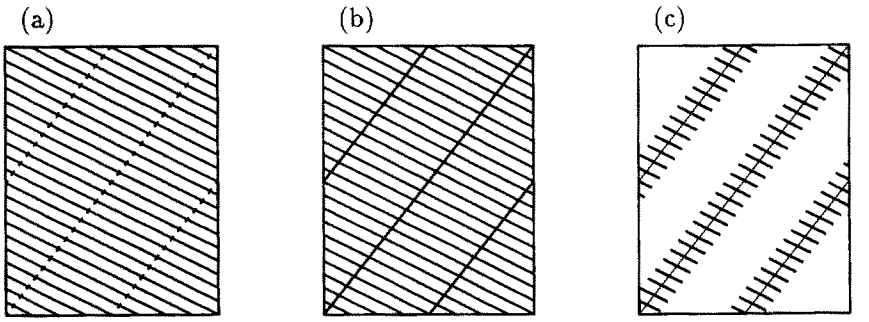

Fig. 9. Typical examples of $EC^{\pm}_{n\tilde{n}kl}$-invariant modes. (a) Just generated. (b) Transient. (c) Echelon mode.

the echelon mode have been initiated by the direct bifurcation and are magnified (damaged) only in the vicinity of the coarse stripes by the secondary bifurcation. On the other hand, the ductile shear zone in Fig. 3 can be understood as an example of the transition mode of Fig. 9(b). The symmetries of the deformation patterns in Figs 1–3 thus can be labeled by the same group $EC^{\pm}_{n\tilde{n}kl}$, regardless of their diversified appearance.

In addition to the diversity in appearance, there exists another source of diversity in echelon modes. As we have seen in Fig. 7, there exists a diversified set of possible $EC^{\pm}_{n\tilde{n}kl}$-invariant bifurcated solutions branching from $OB^{\pm}_{n\tilde{n}}$-invariant stripe pattern solutions. Such diversity will imply the essential complexity of bifurcation behavior of uniform materials.

Uniform materials usually form a $OB_{nn}^{\pm}$-invariant stripe pattern through the direct bifurcation, but $EC_{nnkl}^{\pm}$-invariant bifurcated solutions vary with individual cases depending on the physical and material properties. Naturally different materials have different deformation patterns, but the present theory implies that such a difference in some cases may merely be a difference in the parameters k and l of the same family of $EC_{nnkl}^{\pm}$-invariant bifurcated solutions. The present theory may be a rational clue to untangle the diversity and complexity of echelon modes of various kinds of materials to reach a unified view.

3. THEORY

The direct and some of the secondary bifurcation of the system of equations for uniform materials in a domain of $C_{\infty v} \times \tilde{C}_{\infty v}$ $[\simeq O(2) \times O(2)]$ symmetry is investigated in this section by means of the group-theoretic bifurcation theory. Necessary background can be found, for example, in Sattinger (1979, 1983), Golubitsky and Schaeffer (1985), Golubitsky *et al.* (1988) and Dinkevich (1991).

3.1. *Formulation*

In this subsection we offer a very brief account of the main ideas of the group-theoretic bifurcation analysis. This is intended to be an informal introduction for engineers by avoiding (and sacrificing) the mathematical rigor and sophistication, for which the reader is referred to the standard textbooks cited above. We assume that the deformed state of the material in question is described by a (vector-valued) function $u(x)$, where x is the coordinate of a point in the domain, and that $u(x)$ is subject to a system of governing equations

$$F(u, f) = 0, \tag{10}$$

where f is a real-valued loading parameter and F is a non-linear operator (defined on a certain function space, to which u belongs, and satisfying relevant regularity conditions).

Let G be a (compact) group of transformations acting on x. For example, $G = C_{\infty v} \times \tilde{C}_{\infty v}$ for the cylindrical domain, and the action of G on x is defined by eqns (2)–(4). We denote by $g \cdot x$ the transformation caused by an element g of G. This induces an action of G on u, denoted similarly by $g \cdot u$. If u is a scalar-valued function, for example, this action is given by

$$(g \cdot u)(x) = u(g^{-1} \cdot x).$$

Equation (10) is called equivariant with respect to G if

$$g \cdot F(u, f) = F(g \cdot u, f) \quad \text{for all } g \in G$$

is satisfied. When eqn (10) represents the governing system for a uniform material (soil) in the aforementioned $C_{\infty v} \times \tilde{C}_{\infty v}$-symmetric cylindrical domain, the equivariance condition should be satisfied if, in addition to the geometrical symmetry of the domain, the material property, the particle and pore water distribution, the boundary conditions, the load pattern, etc. have the same symmetry group. It should be understood that the equivariance condition is not an artificial condition for mathematical convenience but a very natural condition, a kind of "objectivity condition", to be satisfied by any physically meaningful mathematical description of symmetric problems.

A solution u is called invariant under G (or G-invariant) if

$$g \cdot u = u \quad \text{for all } g \in G$$

is satisfied. We assume that the solutions (u, f) lying on the main path retain G-invariance, whereas those on a bifurcation path have a reduced symmetry. A reduced symmetry can be labeled by a subgroup G' of G, and u is called G'-invariant if

$$g \cdot u = u \quad \text{for all } g \in G'$$

is satisfied.

Let (u^c, f^c) be a critical point on the main path, at which the derivative (or the Fréchet derivative) of F with respect to u:

$$F'(u, f) = \frac{\partial F}{\partial u}(u, f)$$

has a zero eigenvalue. Note that $F'(u, f)$ reduces to the tangent stiffness matrix or the Jacobian matrix if the system (10) is finite dimensional. A critical point is either the limit point of loading parameter f or a bifurcation point. The bifurcation paths, branching from the main path at a bifurcation point, are usually made up of solutions (u, f) of reduced symmetries, that are to be labeled by subgroups of G.

The multiplicity of a critical point (u^c, f^c) is defined as

$$M = \dim[\ker (F'(u^c, f^c))]$$

[where $\ker(\cdot)$ denotes the kernel space of the linear operator in the parentheses]. The solution (u^c, f^c) is a simple bifurcation point or a multiple point according to whether $M = 1$ or $M \geqslant 2$.

The kernel space $X = \ker (F'(u^c, f^c))$ is easily verified to be invariant under G, i.e.

$$g \cdot u \in X \quad \text{if } u \in X,$$

if u^c is G-invariant. Then the critical point is divided into two types, group-theoretic or parametric, according to whether X is G-irreducible or not. Here X is said to be G irreducible if there exists no non-zero proper subspace in X that is invariant under G. The group-theoretic critical point occurs due to the symmetry of the system while the parametric critical point occurs by the accidental coincidence of two or more critical points. Since the latter is rare, we consider only the former type in the remainder of this paper. Note that a simple critical point is always group-theoretic critical point.

Let (u^c, f^c) be a group-theoretic critical point. Then, by definition, the kernel space X is associated with one of the irreducible representations, which we denote by μ. The irreducible representation, in turn, is associated with a subgroup $G^{(\mu)}$ of G. To be more specific, let $T^{(\mu)}(g)$ $(g \in G)$ be the representation matrices of the irreducible representation μ. Then

$$G^{(\mu)} = \{g \in G \mid T^{(\mu)}(g) = I\},$$

where I is the identity matrix. This subgroup is called the symmetry group of the kernel space. For example, a limit point of the loading parameter f is associated with the unit (one-dimensional) representation μ for which $T^{(\mu)}(g) = 1$ for all $g \in G$, and $G^{(\mu)} = G$. A bifurcation point is usually associated with an irreducible representation μ for which $T^{(\mu)}(g) \neq I$ for some $g \in G$, and hence $G^{(\mu)}$ is a proper subgroup of G. Such a bifurcation point is called a symmetry-breaking bifurcation point. Note that the degree of the irreducible representation is equal to the multiplicity M of the critical point.

The Lyapunov–Schmidt decomposition reduces the original equation to a system of finite-dimensional (bifurcation) equations. Let ϕ_i^c $(i = 1, \ldots, M)$ be the M independent eigenfunctions of the zero eigenvalue at a group-theoretic bifurcation point (u^c, f^c) of multiplicity M. Then we can define an incremental variable $\mathbf{w} = (w_1, \ldots, w_M)^T$ and $\tilde{f}$ from the critical point (u^c, f^c) as:

$$u = \sum_{i=1}^{M} w_i \phi_i^c + u^c, \quad f = f^c + \tilde{f}.$$

Then the bifurcation equation reads

$$\mathbf{F}(\mathbf{w}, \tilde{f}) = \mathbf{0}. \tag{11}$$

When the original equation F is equivariant to G, the bifurcation equation $\mathbf{F}$ can be chosen to be equivariant to G with respect to the associated irreducible representation, that is,

$$\hat{T}(g)\mathbf{F}(\mathbf{w}, \tilde{f}) = \mathbf{F}(\hat{T}(g)\mathbf{w}, \tilde{f}) \quad \text{for all } g \in G, \tag{12}$$

where $\hat{T}(g)$ is the $M \times M$ irreducible representation matrix. It is this inheritance of symmetry to the bifurcation equation that plays a key role in determining possible bifurcating solutions at a critical point. The notation of the symmetry group of the kernel space is vital in the study of the bifurcation structure in that it also labels the symmetry of the eigenfunctions ϕ_i^c. That is, each ϕ_i^c is invariant to the symmetry subgroups associated with the critical point.

3.2. *Bifurcation structure of a* $C_{\infty v}$*-equivariant system*

As a preliminary stage to investigating the bifurcation structure of a $C_{\infty v} \times \tilde{C}_{\infty v}$-equivariant system, we offer here a review on the structure of a $C_{\infty v}$-equivariant system. Recall that both $C_{\infty v}$ and $\tilde{C}_{\infty v}$ are isomorphic to $O(2)$, and therefore have identical bifurcation structures.

We index the family of non-equivalent irreducible representations of $C_{\infty v}$ [$\simeq O(2)$] by

$$R(C_{\infty v}) = \{+, -, 1, 2, \ldots\}. \tag{13}$$

Here $+$ corresponds to the unit (one-dimensional) irreducible representation and $-$ to the other one-dimensional irreducible representation, being defined by the one-dimensional representation matrices

$$T^{(+)}(c(\varphi)) = 1, \quad T^{(+)}(\sigma_Y) = 1, \tag{14}$$

$$T^{(-)}(c(\varphi)) = 1, \quad T^{(-)}(\sigma_Y) = -1, \tag{15}$$

where $T^{(\mu)}(\cdot)$ denotes the representation matrix expressing the action of the element in parentheses. The remaining irreducible representations, labeled $1, 2, \ldots$, in eqn (13) are of degree two, and their actions are defined by

$$T^{(n)}(c(\varphi)) = \begin{pmatrix} \cos(n\varphi) & -\sin(n\varphi) \\ \sin(n\varphi) & \cos(n\varphi) \end{pmatrix}, \quad T^{(n)}(\sigma_Y) = \begin{pmatrix} 1 & 0 \\ 0 & -1 \end{pmatrix}, \quad n = 1, 2, \ldots. \tag{16}$$

We can see from eqns (14)–(16) that

$$G^{(+)} = C_{\infty v}, \quad G^{(-)} = C_{\infty},$$

$$G^{(n)} = C_n, \quad n = 1, 2, \ldots,$$

where C_{∞} and C_n are cyclic groups defined by

Table 1. Irreducible representations $(k, \tilde{k})$ of $C_{\infty v} \times \tilde{C}_{\infty v}$

Degree of $(k, \tilde{k})$	k	$\tilde{k}$
1	+, −	+, −
2	+, −	1, 2, ...
	1, 2, ...	+, −
4	1, 2, ...	1, 2, ...

$$C_\infty = \{c(\varphi) | 0 \leqslant \varphi < 2\pi\},$$

$$C_n = \left\langle c\left(\frac{2\pi}{n}\right) \right\rangle = \left\{ c\left(\frac{2\pi k}{n}\right) \middle| k = 0, 1, \ldots, n-1 \right\}.$$

The group C_n, for example, denotes cyclic symmetries with respect to the circumferential rotation at angles of $2\pi k/n$ $(k = 0, 1, \ldots, n-1)$.

The group $C_{\infty v}$, which represents the (circular) symmetry of the solutions on the main path, is associated with the limit point of loading parameter f, while the subgroups C_∞ and C_n to bifurcation points. The subgroup C_∞, corresponding to a one-dimensional non-unit representation, is associated with a simple, symmetric bifurcation point with a C_∞-invariant bifurcation mode. The subgroup C_n, corresponding to a two-dimensional irreducible representation, is associated with a symmetric,† group-theoretic double bifurcation point, from which C_{nv}-invariant bifurcation paths,‡ with a higher symmetry than C_n, are known to branch (Sattinger, 1983). Here C_{nv} denotes a regular n-gonal symmetry in the circumferential direction, and is defined by

$$C_{nv} = \left\langle \sigma_y, c\left(\frac{2\pi}{n}\right) \right\rangle = \left\{ c\left(\frac{2\pi k}{n}\right), \sigma_Y c\left(\frac{2\pi k}{n}\right) \middle| k = 0, 1, \ldots, n-1 \right\}.$$

A harmonic function $\cos(n\theta)$ is a typical example of C_{nv}-invariant pattern.

To sum up, the deformation modes on the bifurcation paths which branch directly from the $C_{\infty v}$-invariant main path are invariant under either C_∞ or C_{nv} $(n = 1, 2, \ldots)$. The complete rule for further bifurcation from the C_{nv}- and C_n-invariant bifurcation paths has already been given in Ikeda *et al.* (1991).

3.3. *Direct bifurcation of a* $C_{\infty v} \times \tilde{C}_{\infty v}$*-equivariant system*

The direct bifurcation of the $C_{\infty v} \times \tilde{C}_{\infty v}$-invariant cylindrical domain is investigated in this section. Since $C_{\infty v} \times \tilde{C}_{\infty v}$ is a direct product of the two isomorphic groups $C_{\infty v}$ and $\tilde{C}_{\infty v}$, the family of the irreducible representations of $C_{\infty v} \times \tilde{C}_{\infty v}$ is indexed by

$$R(C_{\infty v} \times \tilde{C}_{\infty v}) = \{(k, \tilde{k}) \mid k, \tilde{k} = +, -, 1, 2, \ldots\},$$

where k stands for the irreducible representations of $C_{\infty v}$ and $\tilde{k}$ for those of $\tilde{C}_{\infty v}$. The degree of the irreducible representation $(k, \tilde{k})$ is equal to the product of the degrees of k and $\tilde{k}$, which are either 1 or 2. Hence the degree of $(k, \tilde{k})$ is either 1, 2 or 4, as categorized in Table 1. The multiplicity M of the relevant critical (bifurcation) point is equal to the value of this degree, 1, 2 or 4.

In order to categorize the bifurcation paths and (group-theoretic) bifurcation points of a $C_{\infty v} \times \tilde{C}_{\infty v}$-equivariant system, we refer to the symmetry group $G^{(\mu)}$ for the irreducible

† The definition of symmetric and asymmetric bifurcation points is given in Thompson and Hunt (1973).

‡ It may be noted that the group C_{nv} is isomorphic to a dihedral group, i.e. $C_{nv} \simeq D_n$ by using the conventional notation D_n for dihedral groups.

representation $\mu = (k, \tilde{k})$, the actual forms of which are listed in Table 2. Here n and $\tilde{n}$ denote finite integer numbers and

$$\tilde{C}_{\tilde{n}v} = \left\langle \sigma_Z, t\left(\frac{L}{\tilde{n}}\right)\right\rangle, \quad \tilde{C}_{\tilde{n}} = \left\langle t\left(\frac{L}{\tilde{n}}\right)\right\rangle.$$

It is noteworthy that the symmetries of the bifurcation paths, which are to be determined by solving the bifurcation equation (11), are not necessarily the same as those of the kernel space X as listed in Table 2. The number of bifurcation paths varies drastically with the multiplicity M of a bifurcation point.

3.3.1. *Simple critical points* (M = 1). The four subgroups $G^{(k,\tilde{k})}(k, \tilde{k} = +, -)$ are associated with the one-dimensional irreducible representations, which in turn are associated with simple critical points. As easily seen from the standard results [see, e.g. Sattinger (1979), Golubitsky and Schaeffer (1985), and Golubitsky *et al.* (1988)], the subgroup $G^{(+,+)}$ is related to the limit point of loading parameter f, while the other three to simple, symmetric bifurcation points. The deformation modes on the bifurcation paths for these bifurcation points are invariant under the same group $G^{(\mu)}$ of the kernel space X, that is, invariant under either $C_{\infty v} \times \tilde{C}_\infty$, $C_\infty \times \tilde{C}_{\infty v}$ or $\langle \sigma_Y \sigma_Z, c(\varphi), t(l)\rangle$ as listed in Table 2.

3.3.2. *Double bifurcation points* (M = 2). The subgroups $G^{(+,\tilde{n})}$, $G^{(-,\tilde{n})}$, $G^{(n,+)}$ and $G^{(n,-)}$ are associated with the double points of bifurcation. As is shown in Table 2, the bifurcation paths have higher symmetries than the kernel space X (see Appendix B for the analysis).

For the subgroups $G^{(+,\tilde{n})}$ and $G^{(n,+)}$, symmetry is reduced in one direction but is kept unchanged in another direction; accordingly, all the bifurcation rules for $C_{\infty v}$ presented in the previous section directly hold merely by replacing a group G' by $C_{\infty v} \times G'$ or $G' \times \tilde{C}_{\infty v}$, respectively. The subgroup $G^{(+,\tilde{n})}$, for example, represents the parallel horizontal stripes, and $G^{(n,+)}$ the vertical ones. Symmetry is reduced in both directions for the subgroups $G^{(-,\tilde{n})}$ and $G^{(n,-)}$.

3.3.3. *Bifurcation points of multiplicity four* (M = 4). The subgroup $G^{(n,\tilde{n})}$ is related to the bifurcation points of multiplicity four ($M = 4$), for which symmetry is reduced in both directions. As has been investigated in Murota and Ikeda (1994) [see also Appendix C], there exist three sheets of bifurcated solutions to eqn (11) that are invariant with respect to either $DI_{n\tilde{n}}$ or $OB^{\pm}_{n\tilde{n}}$, defined by eqns (5), (6) and (7). Note that the bifurcated solutions have a higher symmetry than the symmetry of the kernel space, which is labeled by $C_n \times \tilde{C}_{\tilde{n}}$.

The group $DI_{n\tilde{n}}$ represents the symmetry of the classical (harmonic) diamond pattern solutions of Fig. 6(a), which have been obtained by the customary bifurcation analysis. Such solutions form a (two-dimensional) sheet.

Table 2. Symmetry groups $G^{(\mu)}$ of the kernel space X and those of the bifurcation paths of a $C_{\infty v} \times \tilde{C}_{\infty v}$-invariant system

Multiplicity M	Irr. Rep. $(k, \tilde{k})$	Symmetry groups $G^{(\mu)}$ for X	Bifurcation paths
1	$(+, +)$	$C_{\infty v} \times \tilde{C}_{\infty v}$	$C_{\infty v} \times \tilde{C}_{\infty v}$
	$(+, -)$	$C_{\infty v} \times \tilde{C}_\infty$	$C_{\infty v} \times \tilde{C}_\infty$
	$(-, +)$	$C_\infty \times \tilde{C}_{\infty v}$	$C_\infty \times \tilde{C}_{\infty v}$
	$(-, -)$	$\langle \sigma_Y \sigma_Z, c(\varphi), t(l)\rangle$	$\langle \sigma_Y \sigma_Z, c(\varphi), t(l)\rangle$
2	$(+, \tilde{n})$	$C_{\infty v} \times \tilde{C}_{\tilde{n}}$	$C_{\infty v} \times \tilde{C}_{\tilde{n}v}$
	$(-, \tilde{n})$	$C_\infty \times \tilde{C}_{\tilde{n}}$	$\left\langle c(\varphi), \sigma_Y t\left(\frac{L}{2\tilde{n}}\right), \sigma_Z\right\rangle$
	$(n, +)$	$C_n \times \tilde{C}_{\infty v}$	$C_{nv} \times \tilde{C}_{\infty v}$,
	$(n, -)$	$C_n \times \tilde{C}_\infty$	$\left\langle \sigma_Y, t(l), \sigma_Z c\left(\frac{\pi}{n}\right)\right\rangle$
4	$(n, \tilde{n})$	$C_n \times \tilde{C}_{\tilde{n}}$	$DI_{n\tilde{n}}$, $OB^{\pm}_{n\tilde{n}}$

The groups $OB^{\pm}_{n\tilde{n}}$ represent the symmetry of the stripe pattern solutions of Figs 6(b) and (c), which are directed in two different directions parallel to a series of oblique straight lines

$$n\frac{\theta}{2\pi} \pm \tilde{n}\frac{Z}{L} = N, \quad N = 0, \pm 1, \pm 2, \ldots.$$

These solutions form a pair of sheets. These are the only oblique stripe solutions that directly branch from the uniform $C_{\infty v} \times \tilde{C}_{\infty v}$-invariant state and that cannot be directly obtained by the customary bifurcation analysis with non-periodic boundaries.

3.4. *Secondary bifurcation from* $\mathrm{OB}^{\pm}_{n\tilde{n}}$*-invariant paths*

The direct bifurcation paths from a $C_{\infty v} \times \tilde{C}_{\infty v}$-invariant main path have been identified in the previous subsection. These bifurcation paths can undergo further progressive symmetry-breaking bifurcation. In particular, the secondary bifurcation from a $OB^{\pm}_{n\tilde{n}}$-invariant path (corresponding to the oblique parallel stripes) plays a key role in the formation of the echelon mode. We will explain this based on the results of Murota and Ikeda (1994), to which the reader is referred for mathematical details.

The irreducible representations of the group $OB^{\pm}_{n\tilde{n}}$ are either one- or two-dimensional. This implies that the (group-theoretic) bifurcation points are either simple or double with $M = 1$ or 2. The bifurcation equations can be analysed in an analogous manner as in Appendix B.

The solution paths bifurcated from a double point are categorized into two types according to the associated symmetry. The first type has the symmetry labeled by $OB^{\pm}_{m\tilde{m}}$ with m and $\tilde{m}$ being divisors of n and $\tilde{n}$ respectively and satisfying $n/m = \tilde{n}/\tilde{m} \geqslant 2$. Note that $OB^{\pm}_{m\tilde{m}}$ is a proper subgroup of $OB^{\pm}_{n\tilde{n}}$. The second type has the symmetry of $EC^{\pm}_{n\tilde{n}kl}$, defined by eqns (8) and (9). This corresponds to the echelon mode (see Fig. 7). Namely, the echelon mode can appear as a result of the secondary bifurcation

$$C_{\infty v} \times \tilde{C}_{\infty v} \rightarrow OB^{\pm}_{n\tilde{n}} \rightarrow EC^{\pm}_{n\tilde{n}kl}. \tag{17}$$

This is not the only possibility of the emergence of the echelon mode. In addition the secondary bifurcation path of the first type, having the symmetry of $OB^{\pm}_{m\tilde{m}}$ can undergo a further bifurcation to yield a bifurcating branch with symmetry $EC^{\pm}_{m\tilde{m}kl}$, which corresponds also to the echelon mode. Namely, the bifurcation process

$$C_{\infty v} \times \tilde{C}_{\infty v} \rightarrow OB^{\pm}_{n\tilde{n}} \rightarrow OB^{\pm}_{m\tilde{m}} \rightarrow EC^{\pm}_{m\tilde{m}kl} \tag{18}$$

leads also to the formation of the echelon mode. Figure 10 shows a typical example of such processes. It is remarked that the processes in eqns (17) and (18) do not exhaust all possible processes generating the echelon modes.

4. TRIAXIAL COMPRESSION TESTS ON CYLINDRICAL SOIL SPECIMENS

A series of triaxial compression tests on cylindrical (Kawasaki clay) soil specimens with a diameter of 3.5 cm and a height of 8.0 cm were conducted to observe the patterns of wrinkles, shear bands and echelon modes [see Nakano (1993) for details]. To make the specimens as homogeneous as possible, those were isotropically consolidated for 24 h at the consolidation pressure of 3.0 kgf cm^{-2}. Then for each specimen the triaxial compression test with undrained or drained boundaries was carried out under an axial strain-control condition.

The test results for a specimen (with undrained boundaries at an axial strain speed of $\dot{\varepsilon}_a = 2.1 \times 10^{-2}\%$ min^{-1}) are thoroughly investigated through diversified viewpoints. Firstly the deviator stress σ_a and axial strain ε_a relation as in Fig. 11(a) is investigated. The axial strain here is defined as positive in compression. The symbols (○) on this curve denote the

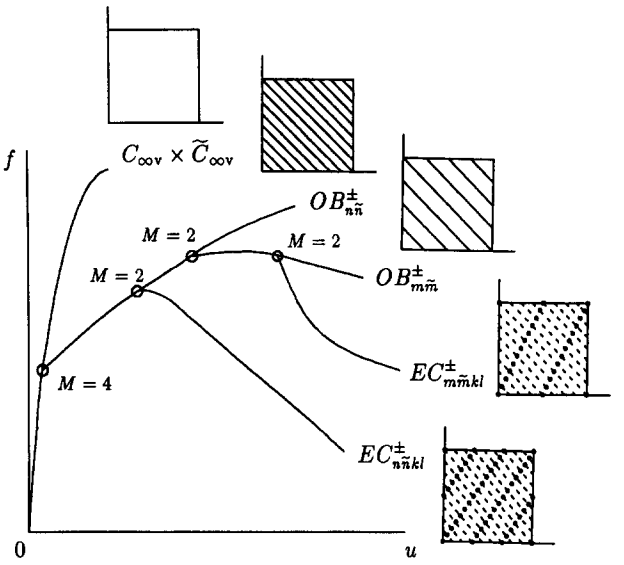

Fig. 10. An example of the emergence of echelon modes through recursive bifurcation (hierarchy). (○): Bifurcation points; M: multiplicity.

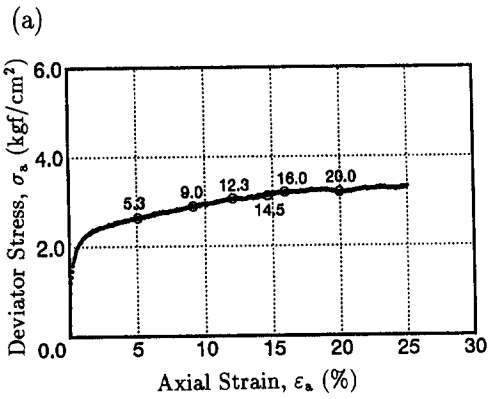

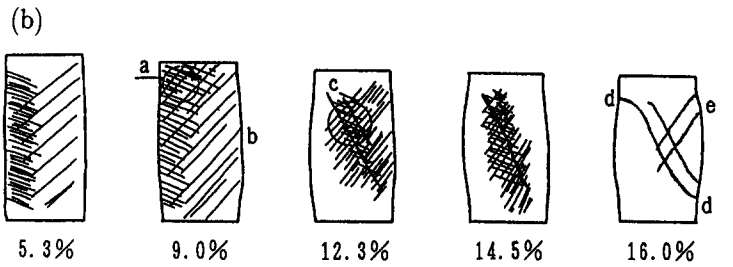

Fig. 11. Results of a triaxial compression test for a cylindrical soil specimen (with undrained boundaries at an axial-strain speed of $\dot{\varepsilon}_a = 2.1 \times 10^{-2}$%/min). (a) Axial deviator stress σ_a versus axial strain ε_a curve; (○): the points at which the deformation patterns were closely observed and illustrated in (b). (b) Sketches of the deformation patterns of the soil specimen.

points at which the deformation patterns were observed closely, as illustrated in Fig. 11(b). During the first stage of the loading ($\varepsilon_a < 1.0\%$), the tangent of the curve is very steep and the specimen is nearly elastic. Its tangent is then greatly reduced during $1.0 < \varepsilon_a < 2.0\%$, and the specimen becomes softened rapidly. It remains fairly constant for $\varepsilon_a > 2.0\%$, and a gradual softening follows. It is slightly reduced at $\varepsilon_a = 20.0\%$, in association with the formation of clear shear plane (band). In the soil mechanics, it is customary (but is to be

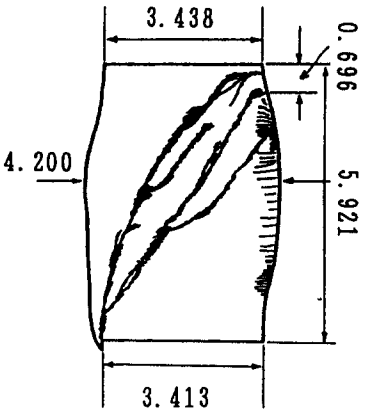

Fig. 12. Sketches of the final stage of the soil specimen taken from behind (unit in cm).

denied by the present theory) to attribute the rapid softening of the curve ($1.0 < \varepsilon_a < 2.0\%$) to the softening of material properties of soils, and the shear band formation ($\varepsilon_a = 20.0\%$) to the direct bifurcation.

Secondly the deformation patterns of the specimen are investigated through a phenomenological standpoint with reference to the sketches in Fig. 11(b). The specimen almost retains its cylindrical shape until $\varepsilon_a = 5.0\%$. At $\varepsilon_a = 5.3\%$ its right-hand side swells to reduce the bilateral symmetry (the loss of the σ_Y-invariance). Moreover, numerous oblique parallel wrinkles emerge on the surface of the specimen. A set of short, parallel wrinkles have a horizontal angle of 10° in the left-hand side, while another set in the left-hand side have an angle of −35° and a greater interval. At $\varepsilon_a = 9.0\%$ a dozen relatively long wrinkles show up in the upper-left part (the zone a), and the right-hand side (the point b) swells significantly. At $\varepsilon_a = 12.3\%$ a pair of distinct wrinkles appear and a large number of wrinkles intersect each other in the center (the zone c) to form an oblique mesh. Some of the wrinkles observed earlier have already disappeared at this stage. At $\varepsilon_a = 16.0\%$ one of the distinct wrinkles becomes less discernible, while the other one is further extended to reach the point d at which the specimen is slightly pinched. The shear plane finally appears at the point e in the upper-right, and develops toward the lower-left to form a number of shear bands. Figure 12 is a sketch of these shear bands taken from behind. The shear bands are made up of a large number of wrinkles that had emerged earlier ($0 < \varepsilon_a < 9.0\%$) but disappeared later ($\varepsilon_a = 12.3\%$). These bands look quite like "echelon", which represents a flight of stairs or wild geese arranged in formation. The progress of the deformation of the specimen is indeed the recursive formation of various kinds of wrinkles directed toward different directions and with different intervals.

Finally these phenomenological features of the deformation of the specimen are theoretically interpreted by means of the present theory. From the sketches shown in Fig. 11(b), one can point out the presence of five deformation patterns in Fig. 13(a), namely, a $C_{\infty v} \times \tilde{C}_{\infty v}$-invariant cylindrical deformation pattern, an $OB^{+}_{n\tilde{n}}$-invariant stripe pattern, an EC^{+}_{nnkl}-invariant transient one of Fig. 9(b), a D_1-invariant pattern for the distinct wrinkle, and a $C_1 \times \tilde{C}_1$-invariant (asymmetric) pattern for the final stage of deformation. Here $D_1 = \langle \sigma_Y \sigma_Z \rangle$ denotes the half rotation symmetry around the center of the specimen (X-axis), and $C_1 \times \tilde{C}_1$ is the trivial subgroup consisting of only one element that leaves everything unchanged. With reference to such change of modes one can predict the occurrence of recursive bifurcation that will trigger the loss of symmetry. Figure 13(b) shows a general view of a σ_a–ε_a curve subject to the recursive bifurcation which is drawn based on this prediction. The shear band formation may be associated with the bifurcation that presumably takes place at one of the last stages of the recursive bifurcation, instead of the direct bifurcation. The mixed presence of different characteristic directions of materials is expected to introduce anisotropies prior to the shear band formation. This may be an essential difficulty in the simulation of shear bands.

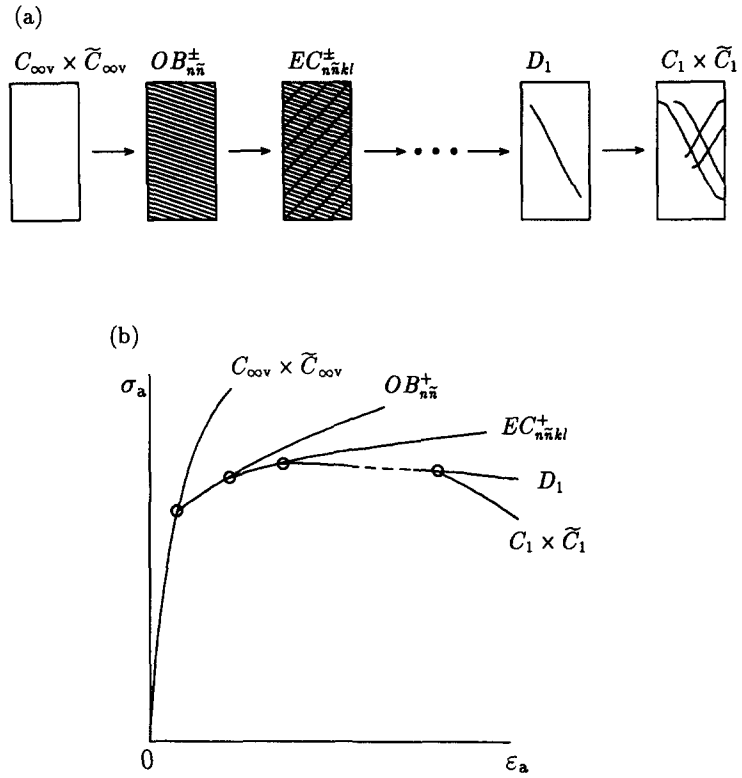

Fig. 13. Recursive bifurcation for the specimen. (a) Recursive loss of symmetry; →: bifurcation process. (b) σ_a-ε_a curve; (○): bifurcation points.

The emergence of the first stripe pattern ($OB^{+}_{n\tilde{n}}$-invariant mode) is the key phenomenon that indicates the occurrence of the direct bifurcation. Since this pattern was already observed at $\varepsilon_a = 5.3\%$, the (direct) bifurcation

$$C_{\infty v} \times \tilde{C}_{\infty v} \rightarrow OB^{+}_{n\tilde{n}}$$

should have taken place prior to $\varepsilon_a = 5.3\%$. It may be a rational hypothesis† that this bifurcation, not the softening of the material properties, has triggered the sharp softening of the ε_a–σ_a curve ($1.0 < \varepsilon_a < 2.0\%$).

Figure 14 shows the sketches of the final configurations of the specimens tested under various kinds of conditions. These configurations are quite diversified; however, they are similar in that they all form echelon or echelon-like modes and display a series of wrinkles directed toward different directions. The deformation patterns in the middle of the specimens that often form "oblique" stripes, especially for Figs 14(d)–(f), are quite different from those in the vicinity of the top and bottom boundaries that form only horizontal stripes. It is these oblique stripes in the middle that have been successfully modeled by the present theory owing to the use of the periodic boundaries in the Z-direction. This may suffice to justify the *infinite cylinder approximation*, which is the major hypothesis of the present theory. Since the triaxial compression tests aim at investigating not the effects of boundaries but the physical properties of soils, it will be more adequate to employ the periodic boundaries in the shear band simulation analysis of soils.

5. CONCLUSIONS

The present theory has clarified the underlying mechanism of the stripe pattern and echelon mode solutions by identifying a sequence of symmetry-breaking bifurcation in eqns (17) and (18) with decreasing symmetries, as illustrated in Fig. 10. The use of the periodic

† A similar hypothesis was presented in Ikeda and Goto (1993).

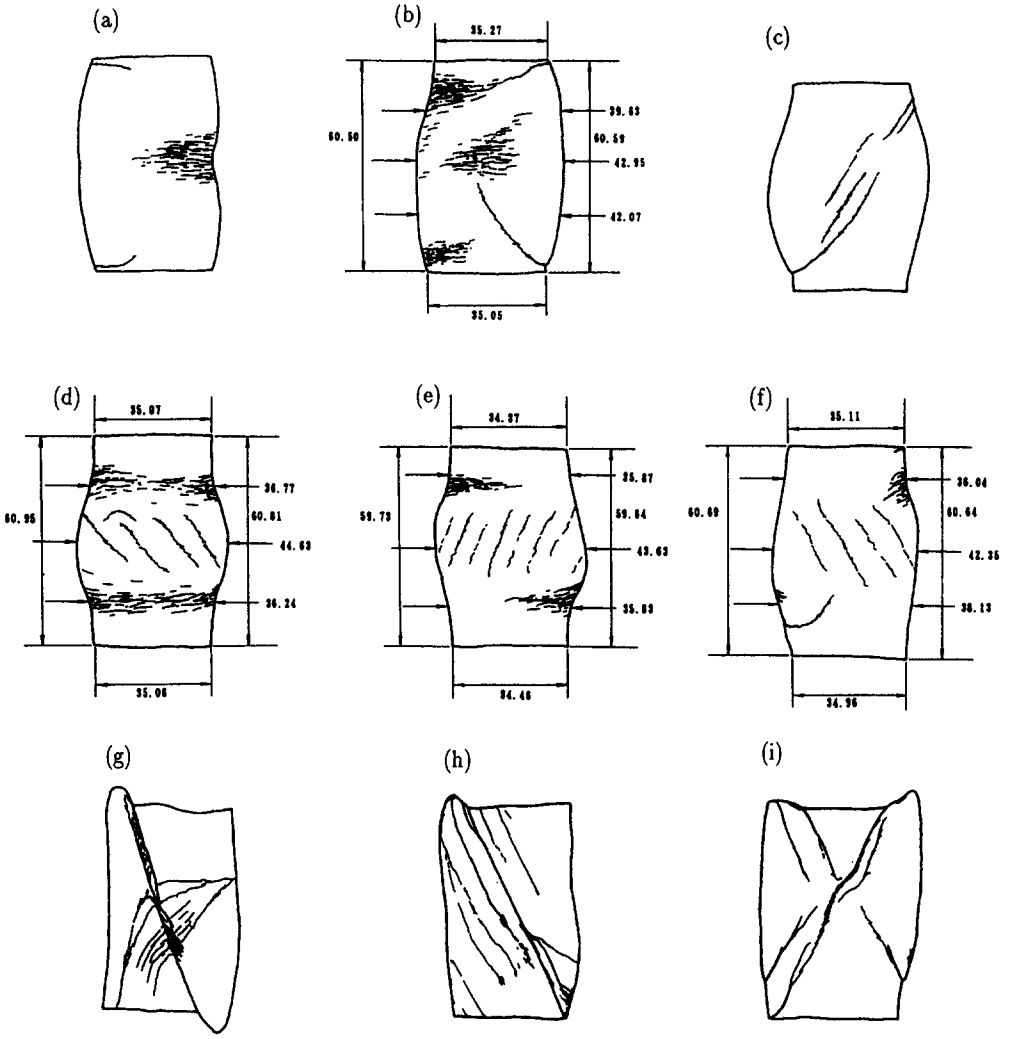

Fig. 14. Sketches of deformation patterns of a series of soil specimens (unit in mm).

boundaries is vital in successfully arriving at the stripe pattern solutions, as has been made clear through the present theory. For ordinary but realistic boundaries, some of the periodic and translational symmetries are lost, and in turn the bifurcation structure has been too simplified to lose these solutions. The cylindrical domain with the ordinary non-periodic boundaries has the reflection symmetry only at the middle ($z = L/2$), and hence is invariant with respect to a group $D_{\infty h} \equiv C_{\infty v} \times \tilde{C}_{1v}$ ($\simeq O(2) \times Z_2$). Since the $OB^{\pm}_{m\tilde{n}}$-invariant stripe pattern solutions are absent in the bifurcation structure for the group $D_{\infty h}$, these solutions cannot be obtained as direct bifurcation from the uniform state. This is an essential difficulty in the customary analysis procedure with non-periodic boundaries. The present theory, revealing the group-theoretic or combinatorial mechanism, gives a clue for overcoming this difficulty. More issues on numerical analysis of echelon modes are treated in Murota and Ikeda (1994).

Acknowledgements—The authors are grateful to Akira Asaoka, Takeshi Tamura and Muneo Hori for shrewd comments, and to Hisashi Okamoto and Makoto Matsumoto for important mathematical information. The discussion with Michael Clausen was instructive for the first author.

REFERENCES

Dinkevich, S. (1991). Finite symmetric systems and their analysis. *Int. J. Solids Structures* **27**(10), 1215–1253.
Golubitsky, M. and Schaeffer, D. G. (1985). *Singularities and Groups in Bifurcation Theory*, Vol. 1. Springer, Berlin.

Golubitsky, M., Stewart, I. and Schaeffer, D. G. (1988). *Singularities and Groups in Bifurcation Theory*, Vol. 2. Springer, Berlin.
Hill, R. and Hutchinson, J. W. (1975). Bifurcation phenomena in the plane tension test. *J. Mech. Phys. Solids* **23**, 239–264.
Ikeda, K. and Goto, S. (1993). Imperfection sensitivity for size effect of granular material. *Soils Foundations* **33**(2), 157–170.
Ikeda, K., Murota, K. and Fujii, H. (1991). Bifurcation hierarchy of symmetric structures. *Int. J. Solids Structures* **27**(12), 1551–1573.
Koschmieder, E. (1974). Benard convection. *Adv. Chem. Phys.* **26**, 177.
Murota, K. and Ikeda, K. (1991). Critical imperfection of symmetric structures. *SIAM J. Appl. Math.* **51**(5), 1222–1254.
Murota, K. and Ikeda, K. (1994). Mathematical mechanism underlying echelon-mode and shear-band formations—bifurcation hierarchy of $O(2) \times O(2)$-equivariant systems, in preparation.
Nakano, M. (1993). Analysis of undrained and partially drained behavior of soils and application to soft clays under embankment loading. Ph.D. thesis (in Japanese). Nagoya University.
Petit, J. P. (1988). Can natural faults propagate under mode II conditions? *Tectonics* **7**(6), 1243–1256.
Prevost, J. H. (1984). Localization of deformations in elastic–plastic solids. *Int. J. Numer. Anal. Meth. Geomech.* **8**, 187–196.
Sattinger, D. H. (1979). *Group Theoretic Methods in Bifurcation Theory*, Lecture Notes in Mathematics 762. Springer, Berlin.
Sattinger, D. H. (1983). *Branching in the Presence of Symmetry*. CBMS-NSF Regional Conference Series in Applied Mathematics 40. SIAM, Philadelphia.
Sekiguchi, H. and Ohta, H. (1977). Induced anisotropy and time dependency of clays. *Proc. Speciality Session* 9. *9th Int. Conf. Soil Mech. Found. Engng*, pp. 229–238.
Shimamoto, T. (1989). The origin of S-C mylonites and a new fault-zone model. *J. Struct. Geol.* **11**(1/2), 51–64.
Taylor, G. I. (1923). Stability of a viscous liquid contained between two rotating cylinders. *Phil. Trans. R. Soc.* **A223**, 289–343.
Thompson, J. M. T. and Hunt, G. W. (1973). *A General Theory of Elastic Stability*. John Wiley, New York.
Vermeer, P. A. (1982). A simple shear-band analysis using compliances. *IUTAM, Conf. Deformation and Failure of Granular Materials*, Balkema, pp. 493–499.
Yamaki, N. (1920). *Elastic Stability of Circular Cylindrical Shells*, Applied Mathematics and Mechanics 27. Elsevier, Amsterdam.
Yatomi, C., Yashima, A., Iizuka, A. and Sano, I. (1989a). General theory of shear bands formation by a non-coaxial Cam-clay model. *Soils Foundations* **29**(3), 41–53.
Yatomi, C., Yashima, A., Iizuka, A. and Sano, I. (1989b). Shear bands formation numerically simulated by a non-coaxial Cam-clay model. *Soils Foundations* **29**(4), 1–13.

APPENDIX A: MODIFICATION FOR RECTANGULAR DOMAINS

The present formulation is applicable also for rectangular domains through a simple modification. We consider the rectangular domain

$$\{(X, Y) \mid 0 \leqslant X \leqslant L_X(f), \quad 0 \leqslant Y \leqslant L_Y(f)\},$$

and employ the "periodically-infinite domain" approximation, that is, the domain has periodic boundaries on the top, bottom, left and right boundaries. Owing to this assumption, the domain has periodic and reflection symmetries in the X- and Y-directions. Such symmetries are labeled by the group $G' = G'_1 \times G'_2$, where G'_1 is generated by

$$t_X(l_X): X \mapsto X + l_X, \quad \sigma_X: X \mapsto -X,$$

where $0 \leqslant l_X < L_X(f)$, and G'_2 by

$$t_Y(l_Y): Y \mapsto Y + l_Y, \quad \sigma_Y: Y \mapsto -Y,$$

where $0 \leqslant l_Y < L_Y(f)$. Note that $G' \simeq G'_1$ and $G_2 \simeq G'_2$ under the correspondence:

$$c(\varphi) \leftrightarrow t_X(l_X) \quad \left(\frac{\varphi}{2\pi} = \frac{l_X}{L_X}\right), \quad \sigma_Y \leftrightarrow \sigma_X;$$

$$t(l) \leftrightarrow t_Y(l_Y) \quad \left(\frac{l}{L} = \frac{l_Y}{L_Y}\right), \quad \sigma_Z \leftrightarrow \sigma_Y.$$

This implies that the rectangular domain can be treated in the same manner as the cylindrical domain, and hence all results of this paper derived for the cylindrical domain are easily extended to such a domain.

APPENDIX B: GROUP-THEORETIC BIFURCATION POINTS OF MULTIPLICITY TWO OF A $C_{\infty v} \times \tilde{C}_{\infty v}$-EQUIVARIANT SYSTEM

We will present the analysis of the bifurcation equation at a group-theoretic bifurcation point of multiplicity two associated with the two-dimensional irreducible representation $(n, -)$ of a $C_{\infty v} \times \tilde{C}_{\infty v}$ $[\simeq O(2) \times O(2)]$-equivariant system. The case for $(-, \tilde{n})$ is similarly obtained. We make use of a slight variant of the standard technique for $O(2)$-equivariant system, which can be found, e.g. in Sattinger (1983), Golubitsky *et al.* (1988), and Murota and Ikeda (1991).

Instead of the real independent variable $\mathbf{w}$ of eqn (11) (with $M = 2$), a complex variable $z = w_1 + iw_2$ is employed, where i denotes the imaginary unit. Then the bifurcation equation (11) takes the form

$$F(\tilde{f}, z) = 0. \tag{B1}$$

It should be clear here that the bifurcated solutions are associated with a particular choice of z that satisfies the bifurcation equation (B1).

We may assume that the action of $C_{\infty v} \times \tilde{C}_{\infty v}$ is defined by

$$\begin{aligned} c(\varphi) &: z \mapsto \omega_n z, \\ \sigma_Y &: z \mapsto \bar{z}, \\ t(l) &: z \mapsto z, \\ \sigma_Z &: z \mapsto -z, \end{aligned} \tag{B2}$$

where $\omega_n = \exp(in\varphi)$ and $\overline{(\cdot)}$ denotes the complex conjugate. Since the group $C_{\infty v} \times \tilde{C}_{\infty v}$ is generated by the four types of elements $[c(\varphi), \sigma_Y, t(l), \sigma_Z]$, the equivariance of the bifurcation equation (11) to the group $C_{\infty v} \times \tilde{C}_{\infty v}$, therefore, is identical with the equivariance under the action of these four types of elements. Namely, the equivariance condition (12) can be rewritten as follows:

$$\omega_n F(\tilde{f}, z) = F(\tilde{f}, \omega_n z), \tag{B3}$$

$$\overline{F(\tilde{f}, z)} = F(\tilde{f}, \bar{z}), \tag{B4}$$

$$-F(\tilde{f}, z) = F(\tilde{f}, -z). \tag{B5}$$

We expand F as

$$F(\tilde{f}, z, \bar{z}) = \sum_{a=0}^{\infty} \sum_{b=0}^{\infty} A_{ab}(\tilde{f}) z^a \bar{z}^b. \tag{B6}$$

(As is usual with local bifurcation analysis, only finitely many terms are important.) The substitution of eqn (B6) into eqns (B3)–(B5) shows that the non-zero terms should satisfy

$$\exp[in\varphi(a-b-1)] = 1, \tag{B7}$$

$$A_{ab}(\tilde{f}) = \overline{A_{ab}(\tilde{f})}. \tag{B8}$$

Since eqn (B7) must hold for an arbitrary value of φ, we have

$$a - b - 1 = 0.$$

With the use of eqn (B7), F in eqn (B6) can be rewritten as

$$F = z \sum_{a=0}^{\infty} A_a(\tilde{f}) |z|^{2a}, \tag{B9}$$

where $A_a(\tilde{f}) = A_{a+1,a}(\tilde{f})$ is real by eqn (B8). Since $(\tilde{f}, z) = (0, 0)$ corresponds to the critical point, we have $A_0(0) = 0$.

The solutions of eqn (B9) are either the trivial solution $z = 0$ or the bifurcated solution, which is to satisfy

$$\sum_{a=0}^{\infty} A_a(\tilde{f}) |z|^{2a} = 0.$$

Hence the bifurcated solution, if any, takes the form $|z| = \Phi(\tilde{f})$.

As the representative of such solutions, we may consider those with z real, because other solutions can be obtained from such solutions by means of transformations by the elements of $C_{\infty v} \times \tilde{C}_{\infty v}$. Then the action (B2) shows that this is invariant to the subgroup generated by

$$\sigma_Y, \sigma_Z c\left(\frac{\pi}{n}\right), \quad t(l).$$

APPENDIX C: GROUP-THEORETIC BIFURCATION POINTS OF MULTIPLICITY FOUR OF A $C_{\infty v} \times \tilde{C}_{\infty v}$-EQUIVARIANT SYSTEM

The solution of the bifurcation equation at a group-theoretic bifurcation point of multiplicity four of a $C_{\infty v} \times \tilde{C}_{\infty v}$ [$\simeq O(2) \times O(2)$]-equivariant system has been obtained by Murota and Ikeda (1994) by adapting the technique for an $O(2) \times SO(2)$-equivariant system described in Sattinger (1983) and Golubitsky *et al.* (1988). We shall reproduce it here for readers' convenience.

Instead of the real independent variable w of eqn (11), complex variables $z_1 = w_1 + iw_2$ and $z_2 = w_3 + iw_4$ are employed. Then the bifurcation equation (11) takes the form

$$F_1(\tilde{f}, z_1, z_2) = F_2(\tilde{f}, z_1, z_2) = 0. \tag{C1}$$

It should be clear here that the bifurcated solutions are associated with the particular choice of z_1 and z_2 that satisfies the bifurcation equation (C1).

The four-dimensional irreducible representation of $C_{\infty v} \times \tilde{C}_{\infty v}$, which is generated by $c(\varphi)$, σ_Y, $t(l)$ and σ_Z, is given by

$$\hat{T}(c) = \begin{bmatrix} \omega_n & 0 & 0 & 0 \\ 0 & \omega_n & 0 & 0 \\ 0 & 0 & \overline{\omega_n} & 0 \\ 0 & 0 & 0 & \overline{\omega_n} \end{bmatrix}, \quad \hat{T}(\sigma_Y) = \begin{bmatrix} 0 & 0 & 0 & 1 \\ 0 & 0 & 1 & 0 \\ 0 & 1 & 0 & 0 \\ 1 & 0 & 0 & 0 \end{bmatrix},$$

$$\hat{T}(t) = \begin{bmatrix} \omega_{\bar{n}} & 0 & 0 & 0 \\ 0 & \overline{\omega_{\bar{n}}} & 0 & 0 \\ 0 & 0 & \overline{\omega_{\bar{n}}} & 0 \\ 0 & 0 & 0 & \omega_{\bar{n}} \end{bmatrix}, \quad \hat{T}(\sigma_Z) = \begin{bmatrix} 0 & 1 & 0 & 0 \\ 1 & 0 & 0 & 0 \\ 0 & 0 & 0 & 1 \\ 0 & 0 & 1 & 0 \end{bmatrix},$$

where $\omega_k = \exp(ik\varphi)$ ($k = n, \bar{n}$; $0 \leqslant \varphi < 2\pi$) and $\overline{(\cdot)}$ means the complex conjugate. Hence we may assume that the action of $C_{\infty v} \times \tilde{C}_{\infty v}$ on (z_1, z_2) is defined by

$$\begin{aligned} c(\varphi)&: z_1 \mapsto \omega_n z_1, \quad z_2 \mapsto \omega_n z_2, \\ \sigma_Y&: z_1 \mapsto \overline{z_2}, \quad z_2 \mapsto \overline{z_1}, \\ t(l)&: z_1 \mapsto \omega_{\bar{n}} z_1, \quad z_2 \mapsto \overline{\omega_{\bar{n}}} z_2, \\ \sigma_Z&: z_1 \mapsto z_2, \quad z_2 \mapsto z_1. \end{aligned} \tag{C2}$$

Since the group $C_{\infty v} \times \tilde{C}_{\infty v}$ is generated by the four elements $[c(\varphi), \sigma_Y, t(l_z), \sigma_Z]$ the equivariance of the bifurcation equation (11) for the group $C_{\infty v} \times \tilde{C}_{\infty v}$, therefore, is identical with the equivariance under the action of these four elements. Namely, the equivariance condition (12) can be rewritten as follows, where the argument $\tilde{f}$ is suppressed for notational simplicity:

$$\begin{aligned} \omega_n F_j(z_1, z_2) &= F_j(\omega_n z_1, \omega_n z_2), & j &= 1, 2, \\ \overline{F_2(z_1, z_2)} &= F_1(\overline{z_2}, \overline{z_1}), & \overline{F_1(z_1, z_2)} &= F_2(\overline{z_2}, \overline{z_1}), \\ \omega_{\bar{n}} F_1(z_1, z_2) &= F_1(\omega_{\bar{n}} z_1, \overline{\omega_{\bar{n}}} z_2), & \overline{\omega_{\bar{n}}} F_2(z_1, z_2) &= F_2(\omega_{\bar{n}} z_1, \overline{\omega_{\bar{n}}} z_2), \\ F_2(z_1, z_2) &= F_1(z_2, z_1), & F_1(z_1, z_2) &= F_2(z_2, z_1). \end{aligned}$$

From these relations we obtain an irredundant set of equivariance conditions as follows:

$$\omega_n F_1(\tilde{f}, z_1, z_2) = F_1(\tilde{f}, \omega_n z_1, \omega_n z_2), \tag{C3}$$

$$\omega_{\bar{n}} F_1(\tilde{f}, z_1, z_2) = F_1(\tilde{f}, \omega_{\bar{n}} z_1, \overline{\omega_{\bar{n}}} z_2), \tag{C4}$$

$$\overline{F_1(\tilde{f}, z_1, z_2)} = F_1(\tilde{f}, \overline{z_1}, \overline{z_2}), \tag{C5}$$

$$F_2(\tilde{f}, z_1, z_2) = F_1(\tilde{f}, z_2, z_1). \tag{C6}$$

We expand F_1 as

$$F_1(\tilde{f}, z_1, z_2, \overline{z_1}, \overline{z_2}) = \sum_{a=0}^{\infty} \sum_{b=0}^{\infty} \sum_{c=0}^{\infty} \sum_{d=0}^{\infty} A_{abcd}(\tilde{f}) z_1^a z_2^b \overline{z_1}^c \overline{z_2}^d. \tag{C7}$$

(As is usual with local bifurcation analysis, only finitely many terms are important.) The substitution of eqn (C7) into eqns (C3)–(C4) shows that the non-zero terms should satisfy

$$\exp[in\varphi(a+b-c-d-1)] = \exp[i\bar{n}\varphi(a-b-c+d-1)] = 1, \tag{C8}$$

$$A_{abcd}(\tilde{f}) = \overline{A_{abcd}(\tilde{f})}. \tag{C9}$$

Since eqn (C8) must hold for an arbitrary value of φ, we have

$$a+b-c-d-1 = a-b-c+d-1 = 0,$$

that is,

$$a-c = 1, \quad b = d. \tag{C10}$$

With the use of eqn (C10), F_1 in eqn (C7) can be rewritten as

$$F_1 = \left[\sum_{a=0}^{\infty}\sum_{b=0}^{\infty} \hat{A}_{ab}(\tilde{f})|z_1|^{2a}|z_2|^{2b}\right]z_1, \tag{C11}$$

where $\hat{A}_{ab}(\tilde{f}) = \hat{A}_{a+1,bab}(\tilde{f})$ is real by eqn (C9). The substitution of eqn (C11) into eqn (C6) leads to

$$F_2 = \left[\sum_{a=0}^{\infty}\sum_{b=0}^{\infty} \hat{A}_{ab}(\tilde{f})|z_1|^{2b}|z_2|^{2a}\right]z_2. \tag{C12}$$

By eqns (C11) and (C12) the bifurcation equation (C1) can be rewritten as

$$\begin{pmatrix} F_1 \\ F_2 \end{pmatrix} = \begin{pmatrix} \left[\sum_{a=0}^{\infty}\sum_{b=0}^{\infty} \hat{A}_{ab}(\tilde{f})|z_1|^{2a}|z_2|^{2b}\right]z_1 \\ \left[\sum_{a=0}^{\infty}\sum_{b=0}^{\infty} \hat{A}_{ab}(\tilde{f})|z_1|^{2b}|z_2|^{2a}\right]z_2 \end{pmatrix} = \mathbf{0}. \tag{C13}$$

Since $(\tilde{f}, z_1, z_2) = (0, 0, 0)$ corresponds to the critical point, we have

$$\hat{A}_{00}(0) = 0.$$

The solutions of eqn (C13) are:

(1) $z_1 = z_2 = 0$,
(2) $z_1 \neq 0, z_2 \neq 0$,
(3) $z_1 \neq 0, z_2 = 0$, or
(4) $z_1 = 0, z_2 \neq 0$.

Those solutions (1)–(4) will turn out to be (1) the trivial; (2) the diamond pattern; and (3)–(4) the two kinds of stripe pattern solutions, respectively.

(1) *Trivial solution* ($z_1 = z_2 = 0$)
The solution $z_1 = z_2 = 0$ corresponds to the trivial solution on the main path with a $C_{\infty v} \times \tilde{C}_{\infty v}$-invariant deformation mode.

(2) *Diamond pattern solution* ($z_1 \neq 0, z_2 \neq 0$)
For $z_1 \neq 0$ and $z_2 \neq 0$, eqn (C13) becomes

$$\begin{pmatrix} \sum_{a=0}^{\infty}\sum_{b=0}^{\infty} \hat{A}_{ab}(\tilde{f})|z_1|^{2a}|z_2|^{2b} \\ \sum_{a=0}^{\infty}\sum_{b=0}^{\infty} \hat{A}_{ab}(\tilde{f})|z_1|^{2b}|z_2|^{2a} \end{pmatrix} = \mathbf{0},$$

the solution of which, if any, is given by

$$|z_1| = |z_2| = \Phi,$$

where Φ is a solution to

$$\sum_{a=0}^{\infty}\sum_{b=0}^{\infty} \hat{A}_{ab}(\tilde{f})\Phi^{2(a+b)} = 0. \tag{C14}$$

Equation (C14) denotes the asymptotic force–displacement relationship $|z_1| = |z_2| = \Phi(\tilde{f})$ for the bifurcated solution. This shows that the branching solutions form a two-dimensional sheet for each $\tilde{f}$.

As the representative of such solutions, we may consider those with $z_1 = z_2$ real, because other solutions can be obtained from such solutions by means of transformations by the elements of $C_{\infty v} \times \tilde{C}_{\infty v}$. Then the action (C2) shows that this is invariant to the subgroup generated by

$$\sigma_Y, \quad \sigma_Z, \quad c\left(\frac{\pi}{n}\right)t\left(\frac{L}{2\tilde{n}}\right), \quad c\left(\frac{\pi}{n}\right)t\left(\frac{-L}{2\tilde{n}}\right).$$

We denote this subgroup by $DI_{n\tilde{n}}$. It is easy to verify that the invariance to this subgroup characterizes a diamond pattern shown in Fig. 6(a).

(3) *Stripe pattern solution* (a) ($z_1 \neq 0, z_2 = 0$)

For $z_1 \neq 0$ and $z_2 = 0$, by eqn (C12) $F_2 = 0$ is always satisfied and $F_1/z_1 = 0$ yields

$$\sum_{a=0}^{\infty} \hat{A}_{a0}(\tilde{f})|z_1|^{2a} = 0,$$

which represents a sheet of asymptotic force–displacement relationship, say, $|z_1| = \Phi(\tilde{f})$ for the bifurcated solution. Among these solutions we may concentrate on those solutions (z_1, z_2) with z_1 real (and $z_2 = 0$), because other solutions can be obtained from such solutions by means of transformations by the elements of $C_{\infty v} \times \tilde{C}_{\infty v}$. We observe here that such solutions with z_1 real are invariant under the transformation by $\sigma_Y\sigma_Z$, and $c(\varphi)t(l)$ with $n(\varphi/2\pi) + \tilde{n}(l/L) = N$ ($N = 0, \pm 1, \pm 2, \ldots$), as is seen from eqn (C2). Thus we have arrived at a $OB^{+}_{n\tilde{n}}$-invariant oblique stripe pattern solution in Fig. 6(b) directed toward the direction parallel with a series of oblique straight lines

$$n\frac{\theta}{2\pi} + \tilde{n}\frac{Z}{L} = N, \quad N = 0, \pm 1, \pm 2, \ldots.$$

(4) *Stripe pattern solution* (b) ($z_1 = 0, z_2 \neq 0$)

The solution $z_1 = 0$ and $z_2 \neq 0$ represents another oblique stripe pattern solution, invariant to $OB^{-}_{n\tilde{n}}$ shown in Fig. 6(c). The stripe pattern is directed toward the direction parallel with another series of oblique straight lines

$$n\frac{\theta}{2\pi} - \tilde{n}\frac{Z}{L} = N, \quad N = 0, \pm 1, \pm 2, \ldots.$$